PASJ: Publ. Astron. Soc. Japan **58**, 335–341, 2006 April 25

Distance Measurement of Spiral Arms in the Galactic-Center Direction Using Radial-Velocity Gradients

Yoshiaki SOFUE
Institute of Astronomy, The University of Tokyo, Mitaka, Tokyo 181-0015
sofue@ioa.s.u-tokyo.ac.jp

(Received 2005 December 6; accepted 2006 January 25)

Abstract

We propose a method to determine the distances of spiral arms in the galactic-center (GC) direction using radial-velocity gradients of approximately straight ridges in longitude–velocity (LV) diagrams of the CO and H I line emissions. We show that the velocity gradient of an LV ridge is uniquely related to the distance. The arms and rings in the central region show large velocity gradients, while nearby arms appear as ridges with small velocity gradients. Applying this method, we determine the distances of the arms on the Sun–GC line, which has remained most difficult in the commonly used kinematical-distance method.

Key words: Galaxy: center — Galaxy: kinematics and dynamics — Galaxy: spiral arms — Galaxy: structure — ISM: H I gas — ISM: molecules

1. Introduction

Longitude–velocity (LV) diagrams of the H I and CO line intensities in the galactic-center (GC) direction have been observed for studying the kinematics and dynamics of interstellar gases in the GC region (Oort 1977; Liszt, Burton 1980; Brown, Liszt 1984; Burton 1988; Bally et al. 1987; Oka et al. 1998; Sofue 1995a; Dame et al. 2001). The diagrams have also been used extensively to derive the gas distribution in the galactic disk and the spiral arms by combining with a rotation curve.

In these studies, however, any distance determinations in the directions of the Sun–GC line have been commonly considered to be most difficult because of the degenerated zero radial velocities. Particularly in CO-line LV diagrams of the GC region (e.g., Bally et al. 1987; Oka et al. 1998), the local and foreground gases appear to be almost horizontal, or slightly inclined narrow ridges in the LV diagrams (LV ridges). These features have been treated as 'contamination' which partially mask and/or obscure the GC features. Figure 1 shows an LV diagram in the ^{12}CO (J = 1–0) line in the GC direction (Oka et al. 1998). The local LV ridges are observed as nearly horizontal, straight features at radial velocities of $-50 < V_{\rm lsr} < 20\,{\rm km\,s^{-1}}$. Some efforts have been devoted to remove the local LV ridges in order to properly study the features associated with the galactic center (Sofue 1995a, b).

While the use of LV diagrams is common for studying the spiral structure of the Milky Way, the distance determination of the arms on the Sun–GC line still remains uncertain. This often causes an erroneous interpretation of interstellar gases, apparently appearing in the GC direction, because of their uncertain distances. In this paper, we propose a method to determine the distances of galactic arms specifically on the Sun–GC. We apply the method to CO and H I LV ridges, and derive the distances to spiral arms. For convenience to use the tabular form rotation curve of the Milky Way given in Sofue et al. (1999), we here assume the rotation velocity and galactocentric distance of the Sun to be $V_0 = 200\,{\rm km\,s^{-1}}$ and $R_0 = 8\,{\rm kpc}$, respectively.

2. The dv/dl Method to Determine the Distances of Inner Arms

2.1. Basic Equations

Suppose that an inner spiral arm or a ring (hereafter an arm) is rotating with the galactic disk between the Sun and GC, and that it appears as an emission or absorption ridge in the CO and H I lines in an LV diagram. We consider the gradient

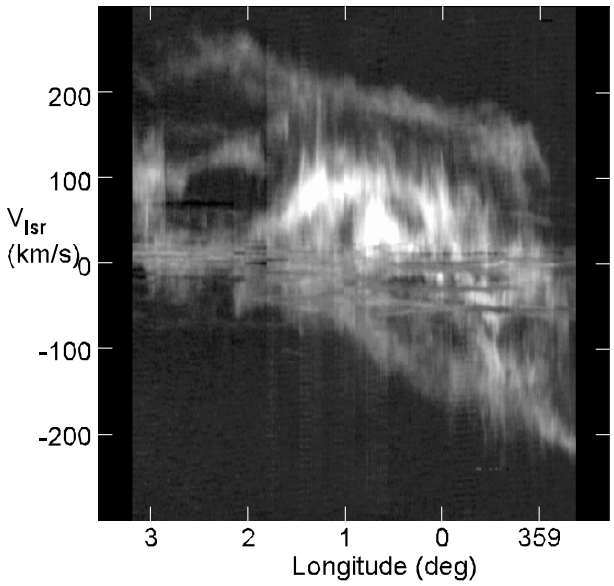

Fig. 1. Longitude–velocity diagram of the ^{12}CO line intensity for the GC region averaged in a latitude range $b = -4'$ to $+4'$ made from a data base by Oka et al. (1998). Note the nearly horizontal, slightly inclined ridges due to the foreground/local arms and rings either in emission or absorption superposed on the high-velocity GC components.

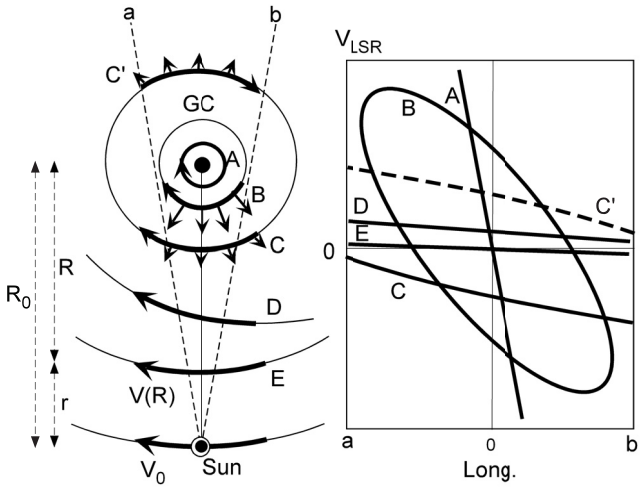

Fig. 2. Correspondence of arms between the GC and Sun with various inclined ridge features in an LV diagram. A, rotating ring near the GC; B, expanding rotating ring; C, the 3-kpc expanding ring/arm; D, spiral arm with non-circular streaming motion; E, circular ring.

dv/dl of the LV ridge, where v is the radial velocity and l is the longitude. Let R and r denote the distance of the arm from the GC and that from the Sun, respectively, and therefore $R + r = R_0$. The galactic disk is rotating at a velocity $V(R)$ at radius R, and the Sun is rotating at $V(R_0) = V_0$. In addition to the circular rotation, we also consider non-circular motion (figure 2).

The radial velocity of a gas element in the galactic plane at galactocentric distance R toward longitude l is expressed by

$$v = R_0(\omega - \omega_0)\sin l = \left(\frac{R_0}{R}V - V_0\right)\sin l, \tag{1}$$

where ω and ω_0 are the angular velocities of the gas and the Sun, and V and V_0 are the rotation velocities at R and R_0, respectively. By differentiating both sides by l we obtain

$$\frac{dv}{dl} = \frac{R_0}{R}(V\cos l - 2Ar\tan p\sin l) - V_0\cos l \tag{2}$$

or

$$R = R_0\left(V_0\cos l + \frac{dv}{dl}\right)^{-1}(V\cos l + 2Ar\tan p\sin l). \tag{3}$$

Here, $A = (V/R - dV/dR)/2$, and p is the pitch angle of the arm corresponding to the LV ridge, whose distance is to be determined. On the Sun–GC line, this equation reduces to

$$R = R_0\frac{V}{V_0}\left(1 \pm \frac{1}{V_0}\frac{dv}{dl}\right)^{-1}, \tag{4}$$

where + and − stand for $l = 0°$ and 180°, respectively. For $V_0 = 200\,\mathrm{km\,s^{-1}}$, we have

$$R = R_0\left(\frac{V}{200\,\mathrm{km\,s^{-1}}}\right)\left(1 \pm 0.286\frac{dv}{dl^\circ}\right)^{-1}\ [\mathrm{kpc}], \tag{5}$$

where dv/dl° is measured in $[\mathrm{km\,s^{-1}\,deg^{-1}}]$.

2.2. *Contributions from Non-Circular and Random Motions*

In the above formulation, we assumed a pure circular rotation. However, the radial velocity, v, is usually superposed by non-circular motions due to expanding motion and/or contracting motion, streaming motion due to a spiral density wave and galactic shock. However, these motions appear as large-scale parallel flow in a small longitudinal segment, and the velocities of these motions are an order of magnitude smaller than that of the galactic rotation. Therefore, their derivatives with respect to l are sufficiently smaller compared to the dv/dl term caused by the galactic rotation.

In addition to the non-circular motions, random velocities due to interstellar turbulence and cloud rotations also affect the dv/dl value. The random-motion term may be given by $dw/dl = r\,dw/dx$, where x is the distance in the cloud. If we take a typical velocity gradient on the order of $\sim 5\,\mathrm{km\,s^{-1}}$ in $\sim 100\,\mathrm{pc}$ by the ISM turbulence, its contribution to dv/dl is only $\sim 0.9\,r/(1\,\mathrm{kpc})\,\mathrm{km\,s^{-1}\,deg^{-1}}$; The nearer is the arm, the smaller is the contribution. It is also negligible for arms near to the GC, where the galactic rotation term is sufficiently large. Thus, we may neglect the contribution by interstellar random motions. We also note that smaller-size clouds, such as cloud cores, may contribute to the velocity gradient, but they are averaged to give a less amount of the velocity gradient.

2.3. *Approximate Distances*

If we assume flat rotation, so that $V = V_0 = 200\,\mathrm{km\,s^{-1}}$, equation (4) gives an approximate distance (figure 3) as

$$R \simeq 8.0\left(1 + 0.286\frac{dv}{dl^\circ}\right)^{-1}\ [\mathrm{kpc}]. \tag{6}$$

For arms near to the GC, where $R \ll R_0$ and $(1/V_0) \times dv/dl \gg 1$, equation (4) can be approximated by

$$R \simeq R_0 V\left(\frac{dv}{dl}\right)^{-1} = 28\left(\frac{V}{200\,\mathrm{km\,s^{-1}}}\right)\left(\frac{dv}{dl^\circ}\right)^{-1}\ [\mathrm{kpc}], \tag{7}$$

where dv/dl° is measured in $[\mathrm{km\,s^{-1}\,deg^{-1}}]$. This equation can be used for distance measurements of arms and rings within $\sim 1\,\mathrm{kpc}$ of the GC. For example, the galactic-center disk within a few hundred pc appears as high-velocity inclined LV features (figure 1), for which $dv/dl^\circ \simeq 200\,\mathrm{km\,s^{-1}\,degree^{-1}}$. Then, we have $R \simeq 0.14\,\mathrm{kpc}$, if $V \sim 200\,\mathrm{km\,s^{-1}}$, which agrees with the radius of the 120 pc molecular ring (Sofue 1995a).

On the other hand, for local arms near the Sun, where $R \simeq R_0$ and $(1/V_0)dv/dl \ll 1$, equation (6) may be reduced to give an approximate value of the distance r from the Sun as

$$r \simeq R_0\frac{1}{V_0}\left(\frac{dv}{dl}\right) = 2.29\left(\frac{dv}{dl^\circ}\right)\ [\mathrm{kpc}]. \tag{8}$$

3. Distances of Galactic Arms on the Sun–GC Line

The distances of arms in the GC direction can be determined by measuring the gradient of LV ridges, dv/dl, and using equation (5). We first calculate an approximate distance R by equation (6) assuming a flat rotation. We then replace V with $V = V(R)$ in equation (5) by using a rotation curve of the Milky Way. By inserting this V, equation (5) yields an iterated

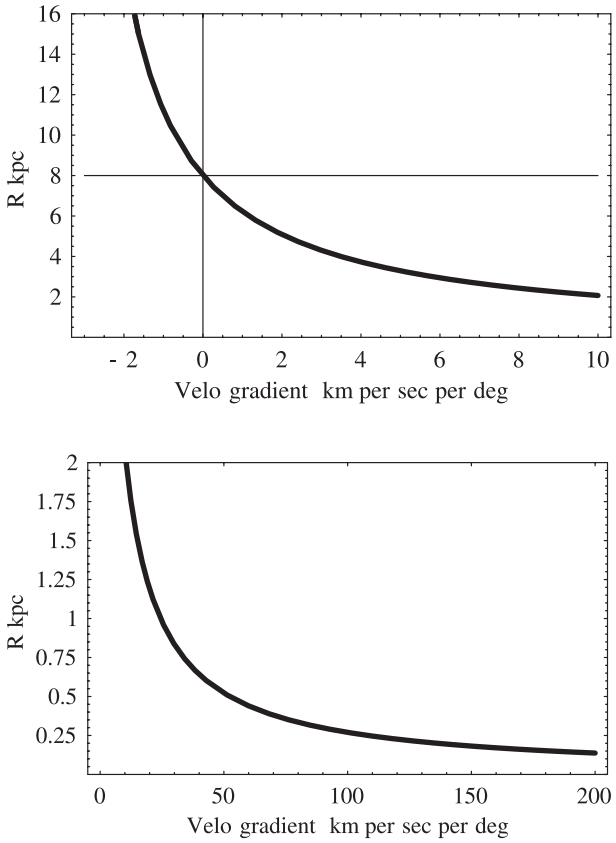

Fig. 3. Upper panel: Galactocentric distance of an arm as a function of dv/dl (in $\mathrm{km\,s^{-1}\,deg^{-1}}$) for a flat rotation with $V = V_0 = 200\,\mathrm{km\,s^{-1}}$ and $R_0 = 8.0\,\mathrm{kpc}$ for small $|dv/dl|$. Lower panel: Same but for large $|dv/dl|$ in the GC region.

$R = R_2$. We then use this new R_2 for the second iterated rotation velocity, $V = V(R_2)$, from the rotation curve, and obtain a third iterated radius, R_3. We repeat this procedure until R_i converges to a stable value.

In figures 4 and 5 we show examples of LV diagrams in the CO line reproduced from Oka et al. (1998) and Dame et al. (1987). We also made use of the CO data from Dame et al. (2001), HI data from Kerr et al. (1981), Westerhout and Wendlandt (1982), and HI data from Burton (1988) for the anti-center direction. Using the LV diagrams, we traced LV ridges and approximated them by straight lines by eye-fitting. In figures 4 and 5, we show the fitted LV straight ridges. Figure 6 shows the fitted LV ridges by straight lines. We measured their values of dv/dl and list them in table 1. Non-circular velocities (velocity offsets) measured at $l = 0°$ are also listed.

Using these measured dv/dl, we derived the distances to corresponding arms. In table 1 we list the obtained R_i, with i being the terminal number of iteration, approximately in the order of the dv/dl values. In the iteration process, we used the rotation curve of Honma and Sofue (1997), which is given in a tabular form in Sofue et al. (1999).

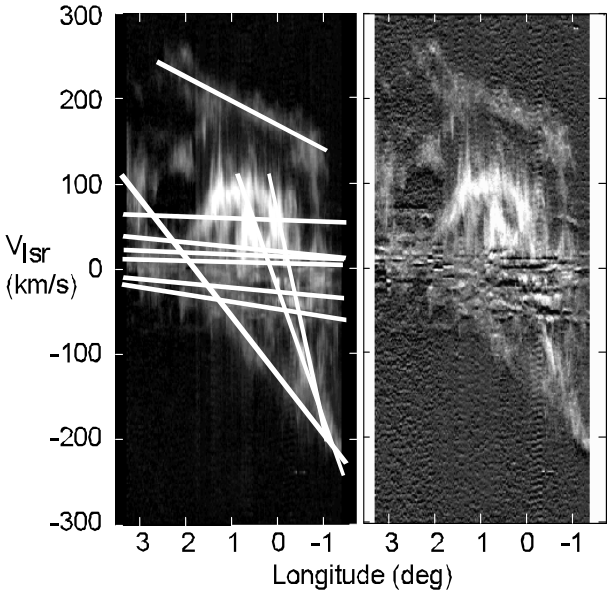

Fig. 4. Left panel: Fitting of LV ridges in the CO-line LV diagram by Oka et al. (1998). Right panel: The same LV diagram, but unsharp-masked in order to enhance the ridges.

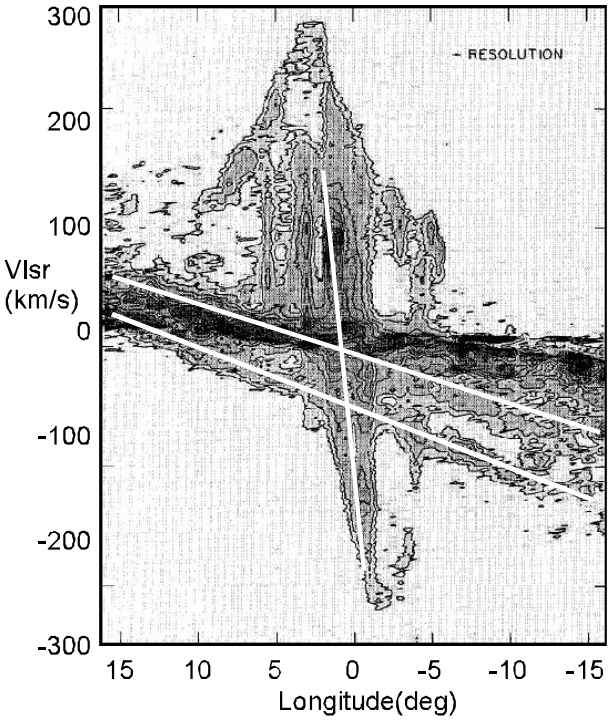

Fig. 5. Fitting of the ridge features in the CO LV diagram by Dame et al. (1987).

3.1. *Identification of Arms*

In table 2 we classify the obtained arms according to their distances from the GC, and identify them with known spiral arms/rings according to the definition of spiral arms in the HI+CO face-on map of the Milky Way (Nakanishi 2005).

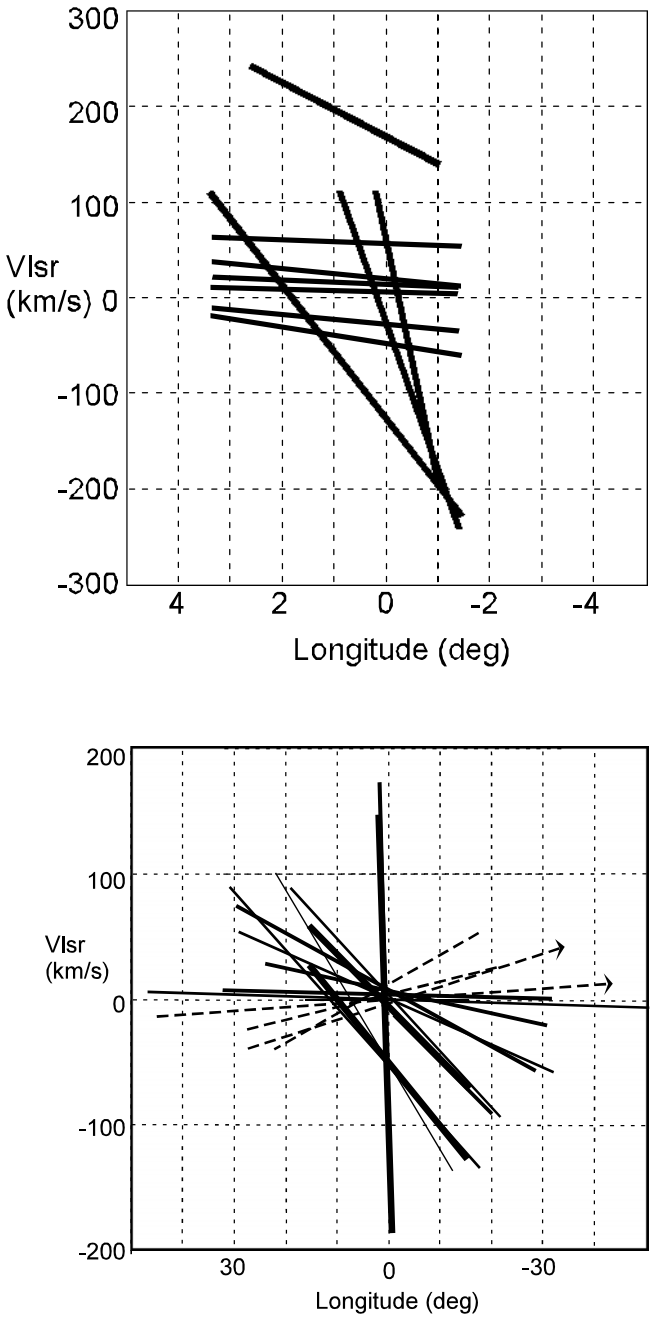

Fig. 6. (a) Upper panel: CO-line LV ridges in the GC direction from the data by Oka et al. (1998). (b) Lower panel: LV ridges for wider area, where thick lines are for the CO-line data by Dame et al. (1987), medium lines for CO data (Dame et al. 2001), thin and thin-dashed arrows for H I data in the GC and anti-center directions, respectively, as taken from H I-line data (Kerr et al. 1981; Westerhout, Wendlandt 1982; Burton 1985).

For several arms, for each of which more than three measured values are available, we calculated the mean values of the radial velocity and galacto centric distance and their standard deviations assuming equal weights for individual measurements.

3.2. Estimates of Errors

Errors in the R determination originate from those in the measured values of dv/dl. The errors in dv/dl of the recognized ridges are caused by the intrinsic velocity dispersion, which is on the order of $10\,\mathrm{km\,s^{-1}}$, and depend on the traced range of the longitude.

For large-scale LV ridges corresponding to the local and intermediate distance arms, the measured longitude ranges are wide, so that errors in dv/dl are on the order of 0.1–$0.2\,\mathrm{km\,s^{-1}\,degree^{-1}}$. This error propagates according to equations (4) and (5) to R as $\delta R \sim 2\delta x$ kpc, where $x = dv/dl^{\circ}$, and hence, the error is approximately $\delta R \sim 0.3$–0.5 kpc. For the GC high-velocity components in the CO-line LV diagrams, the errors are typically $30\,\mathrm{km\,s^{-1}}/3^{\circ} \sim 10\,\mathrm{km\,s^{-1}\,degree^{-1}}$. It propagates via equation (4), yielding $\delta R \sim (28/x)(\delta x/x)$. Since $x \sim 10^2\,\mathrm{km\,s^{-1}\,degree^{-1}}$ for GC, we have $\delta R \sim 30$ pc.

For some identified arms, we have three to four independent measurements of dv/dl and R for each arm. The measured values are deviated around the mean value by the same amount as the measured error as estimated above (± 0.3–0.5 kpc). For these arms, we adopted the mean values and their standard deviations among the measured values with equal weighting as the values of R and δR, and list them in table 2.

The errors caused by the iteration process to obtain R_i depend on the accuracy of the used rotation curve. In so far as the rotation curve is a slowly and smoothly varying function of R, it does not cause an increase in the statistical error. The inner rotation curve within the solar circle at $R < 8$ kpc has been determined with sufficient accuracy of $\delta V_{\rm rot} \sim \pm 5\,\mathrm{km\,s^{-1}}$ (Honma, Sofue 1997). It causes a systematic error in R_i on the order of $\delta R_i/R_i \sim \delta V_{\rm rot}/V_{\rm rot} \sim 0.03$, or $\delta R_i \sim 0.1$–0.2 kpc. This amount of error for the intermediate distance arms is smaller than the statistical errors.

On the other hand, the systematic error in the outer rotation curve at $R > 8$ kpc increases as R increases. This will cause a larger error in R_i. If we take $\delta V_{\rm rot} \sim 20\,\mathrm{km\,s^{-1}}$ for the outer rotation curve (Honma, Sofue 1997), it yields $\delta R_i \sim \pm 1$–2 kpc for $R_i \sim 10$–20 kpc.

4. Discussion

4.1. The Arms on the Sun–GC Line

The obtained R_i values crowd at several values, suggesting that the measured features are not independent features. In fact, they are classified into several groups, as shown in table 2, and each group corresponds to a spiral arm.

GC Rings: LV ridges with large velocity gradient are due to the molecular rings in the GC region. They are rings with 100–200 pc radii, as shown by detailed LV analyses of the CO data (Sofue 1995a, b). In addition to the large velocity gradient, they are often superposed by large non-circular motions on the order of $100\,\mathrm{km\,s^{-1}}$. Such motion may be due to explosive events or non-circular streaming motion in an oval potential. The identified arms in the present method are consistent with the rings discussed in Sofue (1995a).

3 kpc Expanding Ring: The so-called 3-kpc expanding ring (Oort 1977) shows up at R = 2.6–3.5 kpc as mildly tilted LV ridges superposed by radial velocities of $\sim -50\,\mathrm{km\,s^{-1}}$.

Table 1. Galactocentric distances of arms between the GC and Sun.*

$dv/dl°$ ($km\,s^{-1}\,deg^{-1}$)	Radial velocity ($km\,s^{-1}$)	R (kpc)	Iterated R_i (kpc)	$r = 8.0 - R$ (kpc)
CO LV ridges in figure 6a				
1.4	6.5	5.7	$R_4 = 6.5$	2.5
2.1	15	5.0	$R_4 = 5.6$	2.4
5.1	21	3.3	$R_2 = 3.3$	4.7
4.9	−27	3.3	$R_2 = 3.3$	4.7
8.6	47	2.3	$R_2 = 2.3$	5.7
2.0	57	5.1	$R_3 = 5.7$	2.3
152	−30	0.18	$R_4 = 0.28$	7.72
250	60	0.11	$R_5 = 0.15$	7.85
71	−131	0.37	$R_4 = 0.54$	7.46
2.8	170	0.89	$R_4 = 0.26$	7.74
CO and H I LV ridges in figure 6b				
0.10	4.6	7.8	$R_1 = 7.8$	0.2
0.12	0.7	7.7	$R_1 = 7.7$	0.3
0.89	7.5	6.4	$R_6 = 7.1$	0.9
1.82	1.2	5.3	$R_6 = 6.1$	1.9
2.23	8.4	4.9	$R_3 = 5.4$	2.6
4.1	−5.1	3.7	$R_5 = 3.9$	4.1
4.4	4.0	3.5	$R_4 = 3.6$	4.4
4.6	−52	3.5	$R_2 = 3.5$	4.5
4.9	−50	3.3	$R_4 = 3.2$	4.8
6.8	−49	2.7	$R_2 = 2.6$	5.7
−1.1	4.8	11.7	$R_8 = 16$	8
−2.31	13.0	23.6	$R_3 = 24$	8
−0.28	0.4	8.7	$R_3 = 8.4$	0.6
−0.88	8.3	10.7	$R_4 = 13.2$	2.8

* We adopted $R_0 = 8.0$ kpc and $V_0 = 200\,km\,s^{-1}$. For the errors, see the text.

The counter part of this ring with respect to the GC appears as features with positive radial velocities.

Molecular Ring: The arm at $R = 3.3$–3.9 kpc is identified with the so-called 4-kpc molecular ring, which is most clearly seen in the CO-line LV diagram (Dame et al. 2001).

Scutum–Crux Arm: The arm at $R = 5.4$–6.1 kpc is identified with the Scutum–Crux arm defined by Nakanishi (2005) in his face-on map of the Milky Way.

Local/Sagittarius–Carina Arm: The arm at $R = 7.1$–8.4 kpc is a local arm with low radial velocities, and may be part of Sagittarius–Carina Arm. The identification of the local arm is still controversial because of its low velocities comparable to interstellar turbulent motions. However, the crowding of the LV ridges indicates that there exists a definite arm structure in the local galactic region.

Perseus Arm: An outer arm at $R = 13$ kpc may be identified with the Perseus arm, while being slightly shifted to a larger radius. The present arm position is significantly shifted from that defined by Nakanishi (2005).

Outer Arms beyond GC: An outer arm is found located at $R = 16$ kpc, which may be an extension of one of the inner arms. Another outermost arm is found at $R = 24$. At such a large radius, however, the adopted rotation curve, which was extrapolated from the rotation curve by Honma and Sofue (1997) beyond 20 kpc, is not accurate enough, and the result may include a large error.

We have shown that the present dv/dl method makes it possible to define galactic arms on the Sun–GC line and to measure their distances, given a rotation curve. The measurement is possible irrespective of their location outside or inside of the solar circle, or in the GC or anti-center direction. This method is, therefore, complimentary to the commonly used velocity-to-space transformation method by using the radial-velocity field, in which the determination becomes most difficult on the Sun–GC line.

4.2. Radial Flow in the Arms

The dv/dl method can also be used to measure the non-circular radial velocity caused by streaming motions almost directly by measuring the velocity offsets at $l = 0°$ and $180°$. This is a unique characteristic of the method, because the streaming motion is thought to make it inaccurate to determine the position of a gas element from its radial velocity by assuming a circular-rotation velocity field (Burton 1988).

Table 2 shows that most of the identified arms show radial flows. The rings near the GC have non-circular velocities on the order of 30 to 60 $km\,s^{-1}$, suggesting a dynamic gas motion in an oval potential. The well-known expanding

Table 2. Arms in the GC and anti-center directions and their identification with known spiral arms.

Radial velocity ($\mathrm{km\,s^{-1}}$)	Iterated R_i (kpc)	Arm identification*
−30	0.28	GC molecular ring: Arm I (Sofue 1995a)
60	0.15	Arm II
−131	0.54	GC expanding ring
170	0.26	
−52	3.5	
−50	3.2	
−49	2.6	
−27	3.3	
-45 ± 12	3.1 ± 0.4	3-kpc expanding ring
47	2.3	Expanding ring beyond GC
57	5.7	
−5.1	3.9	
4.0	3.6	
21	3.3	
6.6 ± 13	3.6 ± 0.3	4-kpc molecular ring
8.4	5.4	
1.2	6.1	
6.5	6.5	
15	5.6	
7.8 ± 5.6	5.9 ± 0.5	Scutum–Crux arm
7.5	7.1	
0.7	7.7	
4.6	7.8	
0.4	8.4	
3.3 ± 3.4	7.75 ± 0.5	Sagittarius–Carina/Local arm
8.3	13	Perseus arm
4.8	16	Outer arm beyond GC
13.0	24	Outermost arm beyond GC

* Identification with the arms defined in Nakanishi (2005).

feature is measured to have an expansion velocity of 130 to $170\,\mathrm{km\,s^{-1}}$. The identified 3-kpc expanding ring shows an expansion velocity of $45\,\mathrm{km\,s^{-1}}$, and its counter part also appears to be expanding at $\sim 50\,\mathrm{km\,s^{-1}}$.

The 4-kpc molecular ring, in which a large amount of high-density molecular gas is concentrated, associated with various active star-forming regions, is receding from the Sun at $7\,\mathrm{km\,s^{-1}}$. This fact may suggest that the ring is slowly contracting, or it is a part of a dense arm having a galactic-shock flow on the order of $\sim 10\,\mathrm{km\,s^{-1}}$. The same argument applies to the radial motion of $8\,\mathrm{km\,s^{-1}}$ in the Scutum–Crux Arm. The Local or Sagittarius–Carina Arm is rotating almost circularly with a very small receding velocity of $3\,\mathrm{km\,s^{-1}}$.

The three outer arms show positive velocities of 8, 5, and $13\,\mathrm{km\,s^{-1}}$, respectively, indicating outflowing or expanding motions. Since both of the arms in the anti-center and GC directions show outflowing motion, these velocities cannot be attributed to the motion of the Sun. The reverse sense of large-scale radial flow outside of the solar circle may be interpreted as being due to a higher pattern speed than the rotation velocity, so that the gas gains angular momentum from the density waves. Namely, the corotation of the pattern and material rotations may be occurring near the solar circle. If we take a corotation radius of $R_c \sim 8\,\mathrm{kpc}$, then the pattern speed will be about $\Omega_p \sim 200\,\mathrm{km\,s^{-1}}/(8\,\mathrm{kpc}) = 25\,\mathrm{km\,s^{-1}\,kpc^{-1}}$. If the Sun is indeed near the corotation, the question why the local arm has not been well defined would be answered by a weak or no galactic shock wave in the solar neighborhood.

References

Bally, J., Stark, A. A., Wilson, R. W., & Henkel, C. 1987, ApJS 65, 13
Brown, R. L., & Liszt, H. S. 1984, ARA&A, 22, 223
Burton, W. B. 1988, in Galactic and Extragalactic Radio Astronomy, ed. G. L. Verschuur & K. I. Kellermann, 2nd ed (New York: Springer-Verlag), 295
Burton, W. B. 1985, A&AS, 62, 365
Dame, T. M., et al. 1987, ApJ, 322, 706
Dame, T. M., Hartmann, D., & Thaddeus, P. 2001, ApJ, 547, 792
Honma, M., & Sofue, Y. 1997, PASJ, 49, 453
Kerr, F. J., Bowers, P. F., & Henderson, A. P. 1981, A&AS, 44, 63
Liszt, H. S., & Burton, W. B. 1980, ApJ, 236, 779
Nakanishi, H. 2005, PhD Thesis, The University of Tokyo
Oka, T., Hasegawa, T., Sato, F., Tsuboi, M., & Miyazaki, A. 1998, ApJS, 118, 455
Oort, J. H. 1977, ARA&A, 15, 295
Sofue, Y. 1995a, PASJ, 47, 527
Sofue, Y. 1995b, PASJ, 47, 551
Sofue, Y., Tutui, Y., Honma, M., Tomita, A., Takamiya, T., Koda, J., & Takeda, Y. 1999, ApJ, 523, 136
Westerhout, G., & Wendlandt, H. U. 1982, A&AS, 49, 143